Received: 30 July 2021 | Accepted: 8 November 2021

DOI: 10.1002/maco.202112708

ARTICLE

Materials and Corrosion

Corrosion protection properties of poly(4-vinyl pyridine) containing multilayer polymeric coatings on magnesium alloy AZ31

Chayanika Das | **Eleni Kastania** | **Julia Witt** | **Ozlem Ozcan**

Bundesanstalt für Materialforschung und-prüfung (BAM), Berlin, Germany

Correspondence
Ozlem Ozcan, Bundesanstalt für Materialforschung und -prüfung (BAM) Unter den Eichen 87, 12205 Berlin, Germany.
Email: Ozlem.Ozcan@bam.de

Funding information
Alexander von Humboldt-Stiftung

Abstract

The aim of this study is to develop polymeric thin films for corrosion protection of magnesium alloy AZ31. As polymer matrix, poly(4-vinyl pyridine) (P4VP) is selected due to its semiconducting properties and protonic conductivity. Polyacrylic acid is tested as crosslinking layers to improve interfacial adhesion. The macroscopic corrosion properties of the multilayer coatings are investigated by means of electrochemical methods, such as linear sweep voltammetry and electrochemical impedance spectroscopy (EIS), in corrosive media simulating technical and biomedical applications. It is demonstrated that thin multilayer coatings can suppress the corrosion rates of magnesium alloys. To our best knowledge, this is the first demonstration of the use of P4VP as a conducting polymer film with protonic conductivity for corrosion protection of magnesium alloys.

KEYWORDS

AZ31, corrosion protection, intrinsically conducting polymers, magnesium alloys, multilayer coatings

1 | INTRODUCTION

Mg alloys with a high strength-to-weight ratio and good castability are industrially promising lightweight materials for automobile and aircraft applications. Due to their density similar to bone density, Mg alloys are potential candidates for implant materials. However, their commercialization is impeded by their high corrosion susceptibility.[1–4] As Mg has a very negative standard potential, it acts as an anode when coupled with metals having more positive standard potentials. Usually, Mg alloys contain Al, Mn, and trace amount of other metallic impurities. These phase-separated regions when get exposed to corrosive media form local galvanic cells, where the Mg matrix acts as anode and the impurities act as cathodic sites.[3] Thus, the dissolution of Mg dominates as the anodic reaction. Also, the native oxide/hydroxide films provide poor protection against corrosion due to their high reactivity and solubility.[5,6] Even though the dissolution of Mg can be helpful for bone tissue healing when used as an implant material, the dissolution rate should be slower for controlled healing and bone regeneration. Hence, temporary corrosion protection is helpful for biomedical applications of Mg alloys. Because the surface of Mg and its alloys instantaneously reacts after exposure to even atmospheric oxygen, temporary protection is also helpful for preprocessing of technical alloys.

Metallurgical efforts taken to minimize galvanic couples have considerable improvements in the corrosion

properties.[7–10] Deposition of barrier coatings to avoid direct contact of metals to the corroding medium is a cost-effective way to prevent corrosion.[5,6,11–13] Among many other techniques, inorganic phosphate and chromate conversion coatings and sol–gel coatings have been successfully applied to protect surfaces temporarily for biodegradable implants application.[14–26] Creating hydrophobic or superhydrophobic surface coatings using hydrothermal treatments in acidic media was also demonstrated to increase the corrosion resistance of technical alloys.[27–29] Such treatments in aggressive acidic media are challenging to apply to highly oxidation-prone Mg-alloy surfaces. Thus, the development of environmentally friendly coatings is of utmost importance today.[30–33] Up to now the generation of hydrophobic surfaces created by self-assembled layers of silanes have been demonstrated as more benign treatment methods to achieve tunable surface properties.[34,35]

Recently, polymers have gained growing technical interest and have a wide range of nontoxic alternatives to offer.[36–47] Few types of polyesters, polycaprolactone, and polyacrylates have been reported to protect Mg and its alloys temporarily for implant applications.[13,48–50] The incompatible interface of the alloy surface and the polymer could lead to severe degradation of implant integrity. To improve the interfacial properties a conversion layer is usually introduced in between the polymer and the alloy surface. For example, a pretreatment of AZ31 with stearic acid followed by the poly(1,3-trimethylene carbonate) coating showed considerably improved protection.[51] Similarly, polyacrylic acid (PAA) gained importance as a self-healing polymer and was used with poly(ethylene imine) on a cerium-based conversion layer to demonstrate the healing of a scratch on AZ31.[52] In more recent approaches, polypyrole- and polyaniline-based intrinsically conducting polymers (ICPs) are also applied. Their corrosion protection mechanism is yet to be examined.[53–56]

The use of poly(4-vinyl pyridine) (P4VP) as a semiconducting polymer with protonic conductivity was demonstrated in many studies.[57–60] P4VP and a few of its derivatives were studied as corrosion inhibitors for metals like Fe, Cu, and Zn in sulfuric acid and nitric acid with different inhibitor concentrations.[61] Due to the lack of fundamental mechanistic details, this class of polymers is not extensively used and has not yet been applied for corrosion protection of Mg and its alloys. To have a better insight into the corrosion inhibition properties of P4VP, it is important to have knowledge of its properties. The chemical structure of P4VP shows no conjugated backbone, unlike ICPs. Hence, it is unique in its conduction mechanism. When most of the common ICPs conduct electrons through their conjugated backbone, the conductivity of P4VP is due to the pH-dependent protonation and deprotonation of the pyridinic nitrogen.[60] During the corrosion process, the pH of the medium increases and the Mg ions are expected to form stable complexes with P4VP, creating a barrier from the corroding medium (Figure 1).

In this study, we investigated the corrosion protection properties of multilayer P4VP coatings on AZ31. To improve the interfacial adhesion, PAA was introduced as a crosslinker. The corrosion behavior of these polymeric films was studied emphasizing the electrochemical aspects using linear sweep voltammetry (LSV) and electrochemical impedance spectroscopy (EIS). The integrity of the coatings after the electrochemical corrosion was analyzed by means of Fourier-transform infrared spectroscopy (FTIR) and energy-dispersive X-ray spectroscopy (EDX) mapping. The barrier properties were investigated by means of

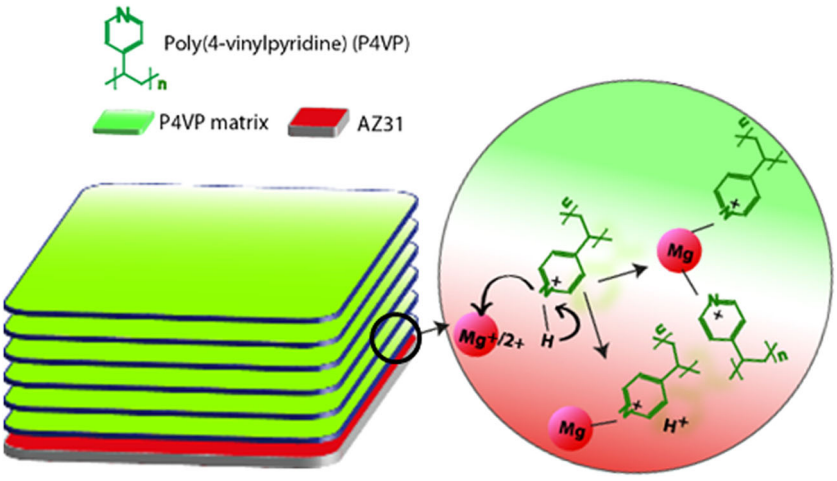

FIGURE 1 Representation of poly(4-vinyl pyridine) (P4VP)- coated AZ31 showing complexation of Mg ions with the pyridinic N of P4VP [Color figure can be viewed at wileyonlinelibrary.com]

immersion studies monitored by a collection of EIS spectra during immersion experiments.

2 | MATERIALS AND METHODS

2.1 | Film preparation

AZ31 Mg alloy (Goodfellow Inc.) was used for all experiments. P4VP (average Mw ~60 000), PAA (average Mw ~100 000, 35 wt% in H_2O), and isopropanol (IPA) were purchased from Sigma-Aldrich and used as received.

AZ31 coupons were ground with 1200-, 2500-, and 4000-grade emery paper and then mirror-polished on the soft polishing pad using 3- and 1-micron diamond paste followed by sonication in IPA for 2 min repeated three times. During the whole process, water was avoided. P4VP (2 mg/ml) was dissolved in IPA. Six layers of P4VP or PAA (1.5 mg/ml in water) were spin-coated on mirror-polished AZ31. The substrates coated with six layers of P4VP and PAA will be referred to as AZ31_$(P4)_6$ and AZ31_$(PA)_6$ throughout the paper, respectively. For mixed-bilayers, PAA and P4VP were spin-coated alternatively. To keep the number of polymer layers constant, three bilayers of PAA/P4VP were spin-coated. The mixed-bilayer films will be referred to as AZ31_$(PA/P4)_3$ throughout the paper. All spin-coated AZ31 substrates were annealed at 100°C for 10 min.

2.2 | Characterization of the multilayer films

The samples were characterized by FTIR spectroscopy, field emission scanning electron microscopy (FESEM), EDX, atomic force microscopy (AFM), and scanning Kelvin probe microscopy (SKPM). FTIR measurements were performed using a Nicolet 8700 (Thermo Fisher Scientific Inc.) spectrometer equipped with a liquid-nitrogen-cooled mercury–cadmium (MCT) detector and a nitrogen-purged measurement chamber with a Veemax III variable-angle specular reflection ATR accessory (Pike Technologies). Spectra were acquired with the angle of incidence set at 70°, with a resolution of 4 cm^{-1}, and averaged over 256 single-beam scans to optimize the signal-to-noise ratio. Spectral acquisition and data processing were managed by the OMNIC 8.1 software package (ThermoElectron Corporation). A VEGA3 TESCAN instrument operated at 20 kV was used to record all the FESEM images. AFM images were recorded with a NanoWizard 4 (JPK Instruments) using silicon cantilevers with a conductive Cr/Pt-coating (Tap300-G: nominal spring constant of 40 N/m) purchased from Budget Sensors, operated in the alternate current (AC) mode with a resolution of 512 × 512 pixels and at a frequency of 0.8 Hz. For the SKPM measurements, an AC voltage of 1 V was applied to the tip and the potential difference between the tip and the surface was recorded. All the AFM and SKP images were analyzed by the JPK Data Processing Suite 6.1.88 software.

2.3 | Electrochemical corrosion and immersion studies

The corrosion behavior of the coated samples was studied electrochemically by means of LSV and EIS. All electrochemical experiments were performed using Gamry Reference 600+ potentiostat/galvanostat/ZRA (Gamry Instruments) and the Gamry Framework data acquisition software (version 7.03), in a typical three-electrode cell where the bare/coated substrate is the working electrode. Phosphate-buffered solution (PBS; pH 7.4, 0.1 M; Chemsolute) was used as an electrolyte in all experiments. Pt wire was used as the counter electrode and Ag/AgCl in 3 M NaCl (manufactured by ALS) was used as the reference electrode. Before the LSV and EIS measurements, open circuit potential (OCP) of the system was monitored for 30 min to attain an equilibrium and ensure a reproducible starting point. The electrode potential was then anodically polarized from −0.5 to +0.5 V with respect to OCP. For immersion experiments, samples were mounted in electrochemical cells, EIS was recorded at OCP in the PBS electrolyte in the frequency range 10^5–0.01 Hz, for 24 h at every 1 h intervals.

3 | RESULTS AND DISCUSSION

The FTIR spectra of AZ31_$(P4)_6$ show peaks at 3066 and 3024 cm^{-1} corresponding to the υ(CH) and 2990 and 2936 cm^{-1} corresponding to $\upsilon_{as}(CH_2)$ and $\upsilon_s(CH_2)$, respectively, arising from the vinyl group (Figure 2a). Figure 2b shows the signature ring vibrations peaks at 1597, 1556, and 1416 cm^{-1} confirming the formation of P4VP films.[62] The AFM topography image of the bare AZ31 (Figure S1a) was characterized by darker polishing lines compared to the AFM image of AZ31_$(P4)_6$ shown in Figure 2c, indicating the formation of thin, smooth, and homogeneous films of P4VP on the AZ31 surface. The AFM images were also recorded at SKPFM mode, which maps the Volta potential difference between the probe and the surface.[63–66] The SKPFM potential images of bare (Figure S1b) and the coated surface (Figure 2d) showed spots of more positive potentials,

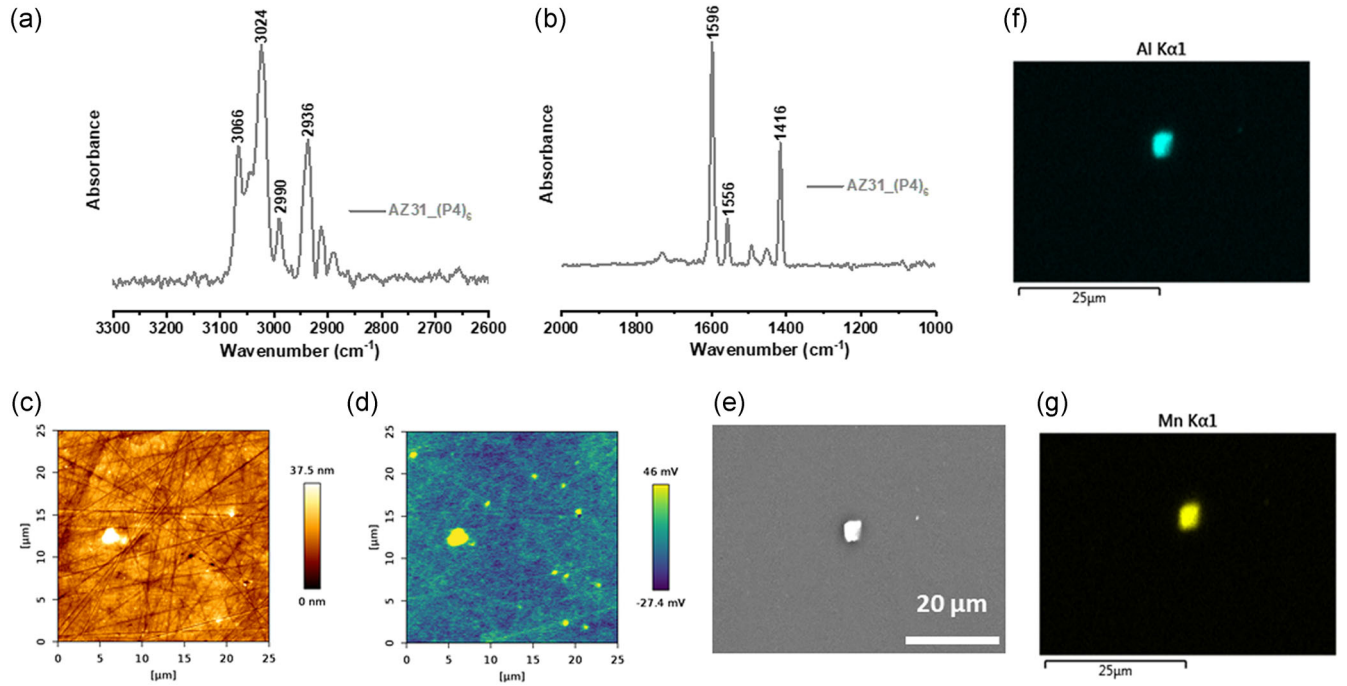

FIGURE 2 Fourier transform infrared spectra of poly(4-vinyl pyridine) showing (a) C–H rocking of the vinyl group and (b) pyridinic ring vibrations; (c) atomic force microscopy image and (d) the corresponding KPM image of the surface of AZ31_$(P4)_6$; (e) field emission scanning electron microscopy image of AZ31_$(P4)_6$, corresponding energy-dispersive X-ray spectroscopy map of AZ31_$(P4)_6$ showing the presence of (f) Al and (g) Mn intermetallic particles [Color figure can be viewed at wileyonlinelibrary.com]

which indicate the presence of the intermetallic particles. These intermetallic particles were also visible in scanning electron microscopy images on AZ31 (Figure S1c) and were confirmed by EDX mapping to be Al-Mn intermetallic particles (Figure S1d,e). The FESEM images of AZ31_$(P4)_6$ confirmed the coating to be homogeneous with the presence of scattered intermetallic particles (Figure 2e). From the EDS mapping, these particles were as well confirmed to be Al-Mn intermetallic particles (Figure 2f,g).

The corrosion protection performance of the spin-coated P4VP layers on AZ31 was investigated electrochemically by means of LSV and EIS measurements in PBS. The Tafel plots in Figure 3a show reduced oxidation and reduction currents for the AZ31_$(P4)_6$ sample in comparison to the bare AZ31 and consequently, the corrosion current (I_{corr}) is also decreased (Table 1). The Nyquist plot of the bare AZ31 shows very low resistance and an inductive loop at the low-frequency region characteristic of Mg (Figure 3b). The Nyquist plot of AZ31_$(P4)_6$ shows higher resistance with a very similar inductive loop at the low-frequency region (Figure 3b). The analysis of the Bode modulus (Figure S2a) and phase (Figure S2a) plots also indicated a higher impedance and a protective effect of AZ31_$(P4)_6$. At low frequencies positive phase angles were also visible in both the Bode phase plots, denoting inductive behavior. The occurrence of the inductive loop is well documented and it has been associated with the relaxation of the charged intermediate species produced due to metal dissolution.[67,68] The presence of monovalent Mg ion is still an ongoing debate.[69] Thus, the appearance of the inductive loop for both AZ31 and AZ31_$(P4)_6$ prompted further investigation of the surfaces after corrosion experiments.

The FTIR spectra of the corroded surfaces of AZ31 and AZ31_$(P4)_6$ showed signals of corrosion products HPO_4^{2-}/PO_4^{3-} and OH^- in the 1200–1000 cm^{-1} and 3600–3200 cm^{-1} regions, respectively (Figure S3). Additionally, the FTIR spectrum of the corroded AZ31_$(P4)_6$ shows the polymer signals both from the vinyl rocking (3100–2900 cm^{-1}) and the ring vibrations (1600–1300 cm^{-1}), suggesting the existence of the polymer coating after the polarization. A closer look at the corroded region under FESEM revealed cracks and cavities formed on the surfaces (Figure S4a). As the corroded regions had a very high surface roughness, AFM analysis was not possible at these regions. When the uncorroded regions were investigated by means of AFM, a dewetting of the polymer film was observed (Figure S4a), which indicated a change in conformation for the polymer layer and consequently the severe corrosion, leading to the formation of defects. The dewetting of the polymer film

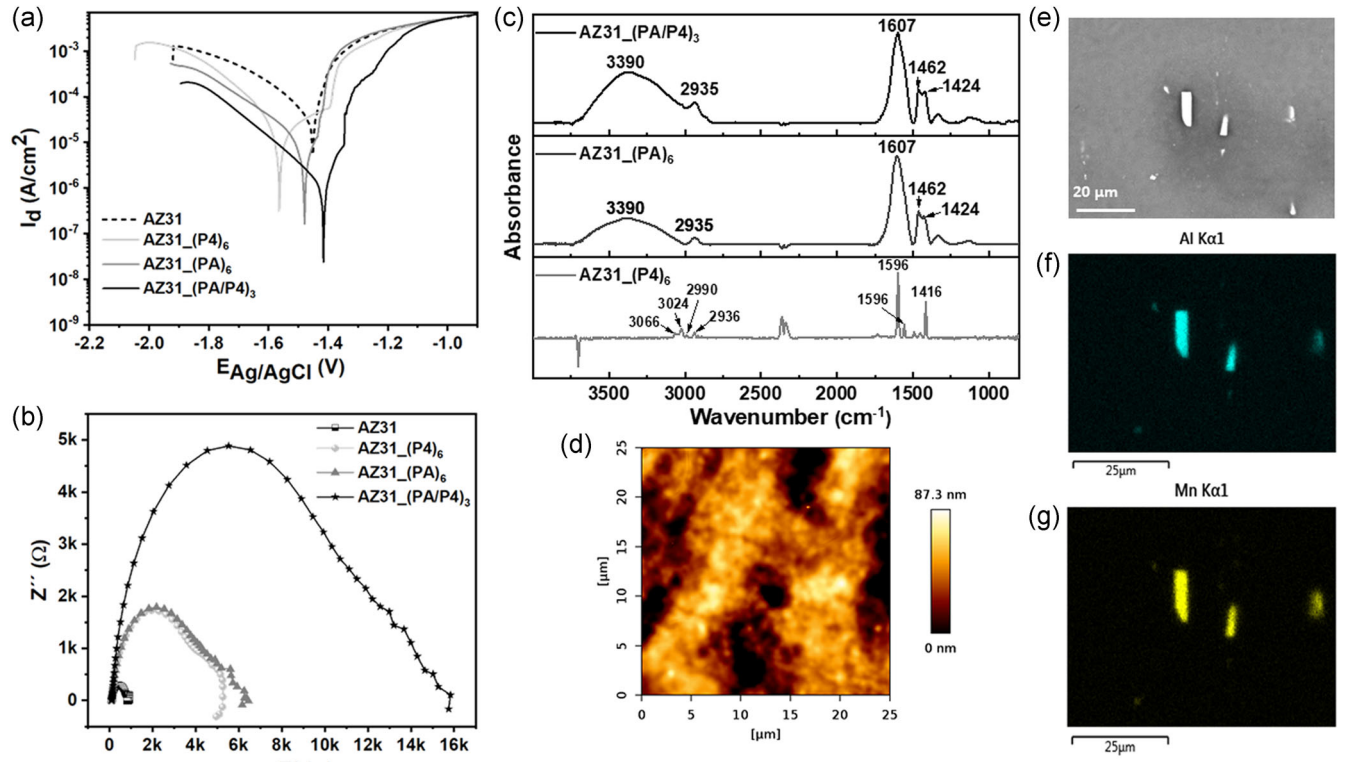

FIGURE 3 (a) Tafel plots and (b) Nyquist plots of AZ31_(PA/P4)$_3$, AZ31_(P4)$_6$, AZ31_(PA)$_6$, and bare AZ31, showing a clear improvement in the corrosion protection property of the polymers and the mixed-bilayer system. (c) Fourier-transform infrared spectra of AZ31_(P4)$_6$, AZ31_(PA)$_6$, and AZ31_(PA/P4)$_3$. (d) Atomic force microscopy topography of AZ31_(PA/P4)$_3$. (e) Field emission scanning electron microscopy image of AZ31_(PA/P4)$_3$ showing particles, which could be intermetallics. (f, g) Energy-dispersive X-ray spectroscopy elemental map confirming the intermetallic particles to be Al-Mn [Color figure can be viewed at wileyonlinelibrary.com]

TABLE 1 I_{corr} values of the studied coating systems and the bare AZ31 sample

Samples	I_{corr} (A/cm^2)
AZ31	4.553×10^{-5}
AZ31_(P4)$_6$	1.288×10^{-5}
AZ31_(PA)$_6$	$6.341 \times 10-^{6}$
AZ31_(PA/P4)$_3$	1.313×10^{-6}

can be a result of poor interfacial adhesion also supported by the appearance of inductive loops in the low-frequency region of the EIS spectra. The carboxylic acid group is known to interact with many other functional groups and so is a potential functionality for crosslinking chemistry. Thus, PAA was chosen as a water-soluble polymer with the carboxylic acid group on each repeating unit as a crosslinker to strengthen the interfacial interaction between the P4VP layers.[52,70] Mixed films of three alternating P4VP and PAA bilayers, AZ31_(PA/P4)$_3$, were prepared and analyzed with the same methodology and six layers of PAA, AZ31_(PA)$_6$, were included in the study for comparison.

The FTIR spectra of AZ31_(PA)$_6$ showed a broad υ(OH) signal at 3390 cm$-^1$, υ(CH$_2$) at 2935 cm^{-1}, υ(C═O) signals at 1607 cm^{-1}, CH$_2$ deformation signal at 1462 cm^{-1}, and υ(CO) coupled with OH$^-$ in-plane bending (Figure 3c).[71,72] The FTIR spectra of AZ31_(PA/P4)$_3$ showed signals from both the polymers; however, the signals from the PAA dominated, and hence, the pyridil ring vibrations in the 1600–1300 cm^{-1} region were suppressed. Very weak signals from the vinyl ring vibrations could be identified in the 3100–2900 cm^{-1} region (Figure S5). In the AFM image of AZ31_(PA/P4)$_3$ and AZ31_(PA)$_6$, no polishing strikes were visible (Figure 3d and S6, respectively) confirming the existence of a thicker coating. The FESEM analysis indicated that homogenous polymer coatings formed for both AZ31_(PA/P4)$_3$ (Figure 3e) and AZ31_(PA)$_6$ (Figure S7a) and the Al/Mn intermetallic particles were still visible under the coatings (Figures 3f,g and S7b,c).

AZ31_(PA/P4)$_3$ was polarized from −0.5 to +0.5 V with respect to OCP and the corresponding Tafel plot was compared to those of AZ31 and AZ31_(P4)$_6$ (Figure 3a). Reduced cathodic and anodic activity, as well as a decrease in I_{corr} by an order of magnitude, was

observed compared to AZ31 and AZ31_$(P4)_6$ (Table 1). To exclude the effect of PAA, the Tafel plot of AZ31_$(PA)_6$ was also compared. The Tafel plot of AZ31_$(PA)_6$ shows very similar characteristics to that of AZ31_$(P4)_6$ with comparable I_{corr} (Figure 3a) values (Table 1). In the Nyquist plot, the semicircle of AZ31_$(PA/P4)_3$ intercepting at the low-frequency region is almost three times as big as that of AZ31_$(P4)_6$ and AZ31_$(PA)_6$ (Figure 3b). Or in other words, the resistance of the mixed films is three times higher than that of the multilayers of individual polymers. The increased resistance was also verified by the Bode modulus plot (Figure S2a). It was also interesting to note the disappearance of the inductive loop in the Nyquist plot in the case of AZ31_$(PA/P4)_3$, as an indication of the inhibition of the dewetting of the thin polymer film and thus slowing down the metal dissolution.

The FTIR spectra of AZ31_$(PA/P4)_3$ and AZ31_$(PA)_6$ after corrosion is similar to that of AZ31_$(P4)_6$ with signals from corrosion products HPO_4^{2-}/PO_4^{3-} and OH^- in the 1200–1000 cm^{-1} and 3600–3200 cm^{-1} region, respectively, along with signals from both the polymers (Figure 3). The uncorroded regions on the AZ31_$(PA/P4)_3$ surface were further investigated by means of AFM. The surface appeared rough with faintly visible polishing strikes and no significant dewetting of the polymers was noticed (Figure S8).

To examine the barrier properties of the polymeric coatings, all coated samples (viz. AZ31_$(PA/P4)_3$, AZ31_$(PA)_6$, and AZ31_$(P4)_6$) were immersed in the PBS solution for 24 h and was monitored every hour by means of EIS. The Bode modulus plots of AZ31_$(PA/P4)_3$ after an hour revealed a similar profile as that of the as-prepared AZ31_$(PA/P4)_3$ with capacitive behavior between high to intermediate frequency followed by a resistance plateau in the low-frequency range, demonstrating the protection effect. Thereafter, a nonperiodical rise and fall of the plateau were noticed. This could be an indication of degradation due to Cl^-, PO_4^{3-}, and reformation of the protective coating by Mg–P4VP complex formation. At a later stage, the resistance plateau of the Bode modulus plot was stabilized. As the lower frequency region gives us valuable information on the protective behavior of the coating, we plotted contour maps of the Bode modulus and phase plots for AZ31_$(PA/P4)_3$ and compared them with other samples (Figure 4a–h). The two key points considered to explicate the Bode contour plots are (i) the higher the resistance in the low-frequency plateau region the better is the protective property of the coating and (ii) positive phase angle indicates the inductive nature of the coating often explained as thinning of the coating or dissolution of the metal.

The modulus contour showing overall impedance at low frequencies in the 24 h time span is highest for AZ31_$(PA/P4)_3$ (Figure 4a). It is observed that for AZ31_$(PA/P4)_3$, initially the impedance is high which after 5 h gradually decreased with time. After 15 h of immersion, a nonperiodic increase and decrease in the impedance were also noticed. For AZ31_$(PA)_6$, impedance was much lower than the mixed-bilayer system, which is almost constant throughout 24 h of immersion with no observable variations (Figure 4b), whereas the AZ31_$(P4)_6$ (Figure 4c) and the bare AZ31 (Figure 4d) have very similar modulus contours. However, when looked carefully, a difference was noticeable at the initial time until

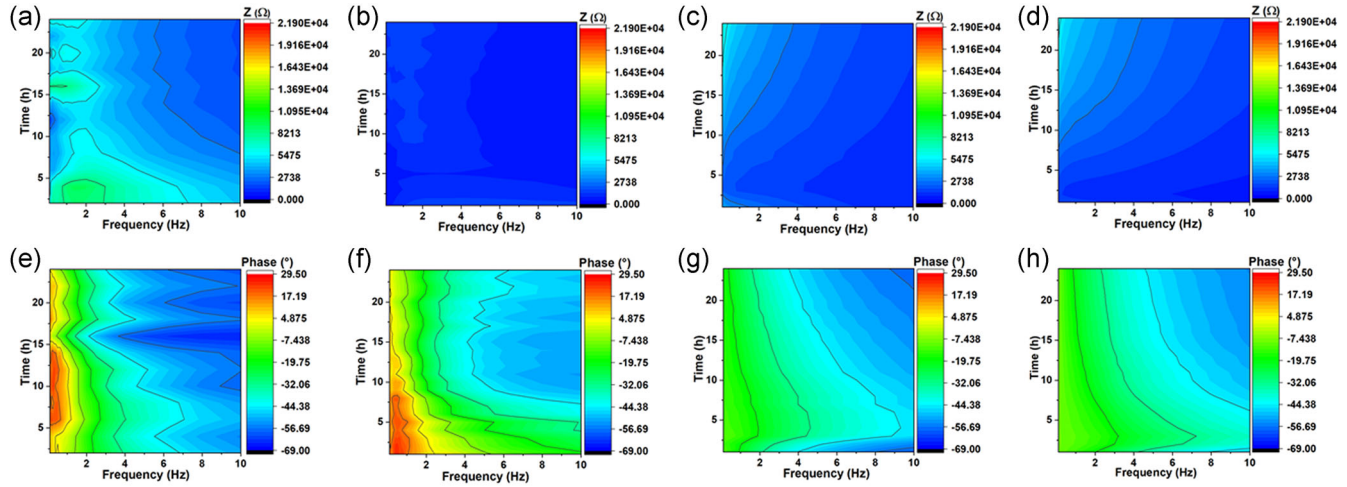

FIGURE 4 Contour representation of Bode modulus plots of (a) AZ31_$(PA/P4)_3$, (b) AZ31_$(PA)_6$, (c) AZ31_$(P4)_6$, (d) AZ31, and the contour representation of Bode phase plots of (e) AZ31_$(PA/P4)_3$, (f) AZ31_$(PA)_6$, (g) AZ31_$(P4)_6$, and (h) AZ31, in the low-frequency region, during the 24-h immersion study [Color figure can be viewed at wileyonlinelibrary.com]

5 h of immersion. Initially, the impedance of AZ31_$(P4)_6$ is slightly higher than that of the bare substrate. After around the seventh hour, the impedance slowly and gradually increased for both systems. Thus, from the modulus contours, it can be inferred that the mixed-bilayer system offers appreciable protection for a longer time span than the AZ31_$(PA)_6$, AZ31_$(P4)_6$, and AZ31. To further investigate the reason behind the nonperiodic increase–decrease of the impedance, the phase contours were examined. The phase contour of AZ31_$(PA/P4)_3$ shows low positive phase angles until 5 h of immersion and high positive phase angles between 5 and 15 h, thereafter again low positive phase angles (Figure 4e). In the case of AZ31_$(PA)_6$, high positive phase angles were observed initially, which gradually faded (Figure 4f). AZ31_$(P4)_6$ and the bare AZ31 have very similar modulus and phase contours (Figure 4g,h); for AZ31_$(P4)_6$, it is explained by the dewetting phenomenon during immersion. Considering the water ingress in the coatings, the delay in the appearance of inductive behavior can be assigned to the improvement of barrier properties. For the AZ31_$(PA/P4)_3$ coatings, the initial protection effect followed by degradation of the film between 5 and 15 h of immersion corroborates the increase in impedance in the same time frame and finally rebuilding of a protective layer possibly by complexing of Mg with P4VP. The occurrence of the inductive behavior on AZ31_$(PA)_6$ initiated earlier than AZ31_$(PA/P4)_3$ and showed a steady degradation of the protective layer. AZ31_$(P4)_6$ and the bare AZ31 showed no sign of inductive loops; however, the low-frequency impedance is consistently low throughout the immersion, indicating very fast corrosion of both the surfaces, so that the defect formation and degradation of the polymer layer were not captured within the time frame of the first EIS measurement, and the capacitive behavior possibly arose due to the growth of the sparingly soluble or insoluble Mg corrosion products. The very fast corrosion rate of the bare AZ31 was an expected finding; however, the similar behavior of AZ31_$(P4)_6$ could be attributed to the dewetting of the polymer surface as mentioned earlier, and hence, again supports the necessity of the mixed-bilayer system for improved interfacial interaction and the controlled release of Mg^{2+}. Considering the overall impedance response and the FESEM analysis, the presence of inductive loops can be assigned to the accumulation of charged intermediate species and consequent growth of corrosion products at the defect areas.

The results of the immersion EIS study agreed with the FESEM analysis (Figure 5). The surface of the AZ31_$(PA/P4)_3$ after 24 h of immersion in PBS had spots of corroded region visible to the naked eye as well as when examined under FESEM (Figure 5a). The corroded region showed severe crack formation (Figure 5b). The uncorroded regions under the FESEM revealed small pits along with unaffected coating areas (Figure 5c). The

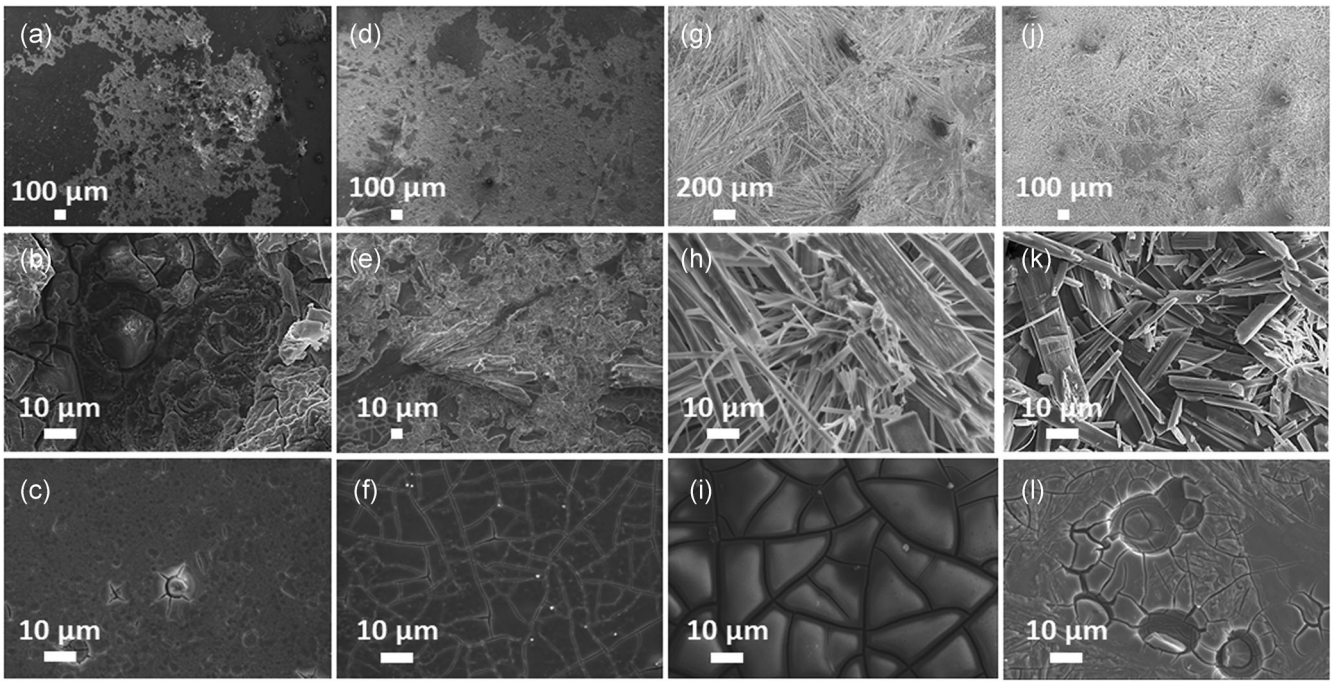

FIGURE 5 Scanning electron microscopy images of (a–c) AZ31_$(PA/P4)_3$, (d–f) AZ31_$(PA)_6$, (g–i) AZ31_$(P4)_6$, and (j–l) AZ31, after 24 h of immersion in phosphate-buffered saline

surface of AZ31_$(PA)_6$ also had patches of corroded regions and uncorroded regions; however, significantly larger corroded regions than that of AZ31_$(PA/P4)_3$ (Figure 5d) showed the presence of crystals of corrosion products (Figure 5e). The uncorroded area appeared to be cracked (Figure 5f). Surfaces of AZ31_$(P4)_6$ and AZ31 showed similar characteristics after 24 h immersion (Figure 5g,h,j,k), with the whole surface covered by crystals. In the case of AZ31_$(P4)_6$, at some regions, the area under the crystals was visible with intensive crack formation (Figure 5h). The cracks were more pronounced on AZ31_$(P4)_6$ surface whereas on AZ31 significant pit formation was observed (Figure 5i,l). The predominant presence of crystals on AZ31_$(P4)_6$ and AZ31 supports their high corrosion rate. The higher corrosion resistance of the mixed-bilayer coatings of PAA and P4VP at short-term immersion was clearly demonstrated.

4 | CONCLUSIONS

P4VP a semiconducting polymer having pH-dependent proton conductivity was studied as a corrosion protection system for Mg alloy AZ31. PAA with a carboxylic acid functional group, a well-known crosslinker, was used to form a polymeric mixed-bilayer coating (AZ31_$(PA/P4)_3$) to improve the interfacial adhesion. Decreased cathodic and anodic activities were observed with the mixed-bilayer films of PAA and P4VP. The Bode contour plots of the low-frequency region also revealed robust protection until 5 h, a decrease of the coating impedance until 15 h, and then a steady behavior of mixed-bilayer coatings. PAA only showed a poor protection effect with gradual decay of the protective layer and the formation of insoluble corrosion products in the later stage of immersion. Thin films of P4VP did not show any improvement of corrosion properties because of the fast dewetting of the polymer from the alloy surface, which occurred within an hour of immersion. The results indicate that mixed-bilayer films of P4VP and PAA are promising candidates for corrosion protection of AZ31 magnesium alloys surfaces.

ACKNOWLEDGMENTS

Part of this study was supported by Alexander von Humboldt-Stiftung, Bonn, Germany, through a Postdoctoral research fellowship of Chayanika Das. Chayanika Das also conveys her sincere thanks to Adolf Martens Postdoctoral Fellowship of The Federal Institute for Material Research and Testing (BAM). The authors also acknowledge Michaela Buchheim and Christiane Weimann for the SEM and EDX measurements.

CONFLICT OF INTERESTS

The authors declare that there are no conflict of interests.

AUTHOR CONTRIBUTIONS

Chayanika Das was involved in conceptualization, investigation (lead), formal analysis, visualization, writing—original draft, and editing. Eleni Kastania and Julia Witt contributed to the investigation and formal analysis. Ozlem Ozcan was involved in supervision, writing, review, and editing.

DATA AVAILABILITY STATEMENT

The data that support the findings of this study are available from the corresponding author upon reasonable request.

ORCID

Ozlem Ozcan http://orcid.org/0000-0002-7457-4985

REFERENCES

[1] M. Esmaily, J. E. Svensson, S. Fajardo, N. Birbilis, G. S. Frankel, S. Virtanen, R. Arrabal, S. Thomas, L. G. Johansson, *Prog. Mater. Sci.* **2017**, *89*, 92.
[2] G. Song, A. Atrens, *Adv. Eng. Mater.* **2003**, *5*, 837.
[3] G. L. Song, A. Atrens, *Adv. Eng. Mater.* **1999**, *1*, 11.
[4] R.-C. Zeng, J. Zhang, W.-J. Huang, W. Dietzel, K. U. Kainer, C. Blawert, W. Ke, *Trans. Nonferrous Met. Soc. China* **2006**, *16*, s763.
[5] S. Feliu, Jr., J. C. Galvan, A. Pardo, M. C. Merino, R. Arrabal, *Open Corros. J.* **2010**, *3*, 80.
[6] Y. C. Wang, B. Y. Liu, X. A. Zhao, X. H. Zhang, Y. C. Miao, N. Yang, B. Yang, L. Q. Zhang, W. J. Kuang, J. Li, E. Ma, Z. W. Shan, *Nat. Commun.* **2018**, *9*, 1.
[7] N. Hort, Y. D. Huang, K. U. Kainer, *Adv. Eng. Mater.* **2006**, *8*, 235.
[8] B. L. Mordike, *Mater. Sci. Eng. A* **2002**, *324*, 103.
[9] M. O. Pekguleryuz, A. A. Kaya, *Adv. Eng. Mater.* **2003**, *5*, 866.
[10] W. Xu, N. Birbilis, G. Sha, Y. Wang, J. E. Daniels, Y. Xiao, M. Ferry, *Nat. Mater.* **2015**, *14*, 1229.
[11] S. Agarwal, J. Curtin, B. Duffy, S. Jaiswal, *Mater. Sci. Eng. C, Mater. Biol. Appl.* **2016**, *68*, 948.
[12] F. H. Cao, J. L. Cao, Z. Zhang, J. Q. Zhang, C. N. Cao, *Mater. Corros.* **2007**, *58*, 676.
[13] R. G. Hu, S. Zhang, J. F. Bu, C. J. Lin, G. L. Song, *Prog. Org. Coat.* **2012**, *73*, 129.
[14] K. Brunelli, M. Dabala, I. Calliari, M. Magrini, *Corros. Sci.* **2005**, *47*, 989.
[15] K. Z. Chong, T. S. Shih, *Mater. Chem. Phys.* **2003**, *80*, 191.
[16] H. H. Elsentriecy, H. M. Luo, H. M. Meyer, L. L. Grado, J. Qu, *Electrochim. Acta* **2014**, *123*, 58.
[17] H. H. Elsentriecy, J. Qu, H. M. Luo, H. M. Meyer, C. Ma, M. F. Chi, *Thin Solid Films* **2014**, *568*, 44.
[18] A. F. Galio, S. V. Lamaka, M. L. Zheludkevich, L. F. P. Dick, I. L. Muller, M. G. S. Ferreira, *Surf. Coat. Technol.* **2010**, *204*, 1479.
[19] Y. P. Li, C. H. Tan, G. W. Qi, J. Guo, X. Wang, S. Y. Zhang, *Corros. Sci.* **2013**, *70*, 229.

[20] Y. Song, S. X. Zhang, J. A. Li, C. L. Zhao, X. N. Zhang, *Acta Biomater.* **2010**, *6*, 1736.
[21] R. C. Zeng, F. Zhang, Z. D. Lan, H. Z. Cui, E. H. Han, *Corros. Sci.* **2014**, *88*, 452.
[22] L. A. Hernández-Alvarado, L. S. Hernández, J. Garrido, S. Rivera-Villalobos, M. L. Escudero, *Surf. Coat. Technol.* **2017**, *325*, 473.
[23] A. Madhankumar, E. Thangavel, S. Ramakrishna, I. B. Obot, H. C. Jung, K. S. Shin, Z. M. Gasem, H. Kim, D.-E. Kim, *RSC Adv.* **2014**, *4*, 24272.
[24] M. Peron, A. Bin Afif, A. Dadlani, F. Berto, J. Torgersen, *Surf. Coat. Technol.* **2020**, *395*, 125922.
[25] C. Wen, S. Guan, L. Peng, C. Ren, X. Wang, Z. Hu, *Appl. Surf. Sci.* **2009**, *255*, 6433.
[26] A. Zaffora, F. Di Franco, D. Virtù, F. Carfì Pavia, G. Ghersi, S. Virtanen, M. Santamaria, *ACS Appl. Mater. Interfaces* **2021**, *13*, 12866.
[27] C.-S. Hsu, M. H. Nazari, Q. Li, X. Shi, *Mater. Chem. Phys.* **2019**, *225*, 426.
[28] M. Liang, Y. Wei, L. Hou, H. Wang, Y. Li, C. Guo, *J. Alloys Compd.* **2016**, *656*, 311.
[29] Z. Wang, Q. Li, Z. She, F. Chen, L. Li, X. Zhang, P. Zhang, *Appl. Surf. Sci.* **2013**, *271*, 182.
[30] D. Balgude, A. Sabnis, *J. Sol-Gel Sci. Technol.* **2012**, *64*, 124.
[31] L. Gao, C. Zhang, M. Zhang, X. Huang, X. Jiang, *J. Alloys Compd.* **2009**, *485*, 789.
[32] C. A. Huang, T. H. Wang, T. Weirich, V. Neubert, *Corros. Sci.* **2008**, *50*, 1385.
[33] S. A. Salman, M. Okido, *Anodization of Magnesium (Mg) Alloys to Improve Corrosion Resistance*, Elsevier, Amsterdam **2013**, pp. 197.
[34] V. K. Korrapati, N. Scharnagl, D. Letzig, M. L. Zheludkevich, *Corros. Sci.* **2020**, *169*, 108619.
[35] A. Zomorodian, F. Brusciotti, A. Fernandes, M. J. Carmezim, T. Moura e Silva, J. C. S. Fernandes, M. F. Montemor, *Surf. Coat. Technol.* **2012**, *206*, 4368.
[36] M. Halik, H. Klauk, U. Zschieschang, G. Schmid, W. Radlik, W. Weber, *Adv. Mater.* **2002**, *14*, 1717.
[37] S. G. Im, P. J. Yoo, P. T. Hammond, K. K. Gleason, *Adv. Mater.* **2007**, *19*, 2863.
[38] S. L. Johnson, H. K. Park, R. F. Haglund, *Appl. Surf. Sci.* **2007**, *253*, 6430.
[39] Y. J. Xia, K. Sun, J. Y. Ouyang, *Adv. Mater.* **2012**, *24*, 2436.
[40] L. Xu, W. Chen, A. Mulchandani, Y. Yan, *Angew. Chem. Int. Ed. Engl.* **2005**, *44*, 6009.
[41] B. Harnish, J. T. Robinson, Z. C. Pei, O. Ramstrom, M. D. Yan, *Chem. Mater.* **2005**, *17*, 4092.
[42] J. Raczkowska, Y. Stetsyshyn, K. Awsiuk, J. Zemla, A. Kostruba, K. Harhay, M. Marzec, A. Bernasik, O. Lishchynskyi, H. Ohar, A. Budkowski, *RSC Adv.* **2016**, *6*, 87469.
[43] F. Brusciotti, D. V. Snihirova, H. Xue, M. F. Montemor, S. V. Lamaka, M. G. S. Ferreira, *Corros. Sci.* **2013**, *67*, 82.
[44] A. S. Hoffman, *Adv. Drug Deliv. Rev.* **2013**, *65*, 10.
[45] C. Janiak, *Dalton Trans.* **2003**, 2781.
[46] W. Sokolowski, A. Metcalfe, S. Hayashi, L. Yahia, J. Raymond, *Biomed. Mater.* **2007**, *2*, S23.
[47] J. L. West, J. A. Hubbell, *React. Polym.* **1995**, *25*, 139.
[48] A. Zomorodian, M. P. Garcia, T. Moura e Silva, J. C. S. Fernandes, M. H. Fernandes, M. F. Montemor, *Mater. Sci. Eng. C* **2015**, *48*, 434.
[49] A. Zomorodian, I. A. Ribeiro, J. C. S. Fernandes, A. C. Matos, C. Santos, A. F. Bettencourt, M. F. Montemor, *Int. J. Polymer. Mater. Polymer. Biomater.* **2017**, *66*, 533.
[50] A. Zomorodian, C. Santos, M. J. Carmezim, T. M. Silva, J. C. S. Fernandes, M. F. Montemor, *Electrochim. Acta* **2015**, *179*, 431.
[51] Y. Li, S. Zhao, S. Li, Y. Ge, R. Wang, L. Zheng, J. Xu, M. Sun, Q. Jiang, Y. Zhang, H. Wei, *Small* **2019**, *15*, 1904486.
[52] F. Fan, C. Zhou, X. Wang, J. Szpunar, *ACS Appl. Mater. Interfaces* **2015**, *7*, 27271.
[53] A. F. Baldissera, C. A. Ferreira, *Prog. Org. Coat.* **2012**, *75*, 241.
[54] P. P. Deshpande, N. G. Jadhav, V. J. Gelling, D. Sazou, *J. Coat. Technol. Res.* **2014**, *11*, 473.
[55] D. E. Tallman, Y. Pae, G. P. Bierwagen, *Corrosion* **1999**, *55*, 779.
[56] M. C. Turhan, M. Weiser, H. Jha, S. Virtanen, *Electrochim. Acta* **2011**, *56*, 5347.
[57] J. Li, I. M. Khan, *Macromolecules* **1993**, *26*, 4544.
[58] S. Maria, A. S. Susha, M. Sommer, D. V. Talapin, A. L. Rogach, M. Thelakkat, *Macromolecules* **2008**, *41*, 6081.
[59] H. T. Pu, *Polym. Int.* **2003**, *52*, 1540.
[60] J. Ruokolainen, R. Makinen, M. Torkkeli, T. Makela, R. Serimaa, G. Brinke, O. Ikkala, *Science* **1998**, *280*, 557.
[61] S. A. Umoren, *Open Corros. J.* **2009**, *2*, 175.
[62] E. Groppo, M. J. Uddin, O. Zavorotynska, A. Damin, J. G. Vitillo, G. Spoto, A. Zecchina, *J. Phys. Chem. C* **2008**, *112*, 19493.
[63] F. Andreatta, I. Apachitei, A. A. Kodentsov, J. Dzwonczyk, J. Duszczyk, *Electrochim. Acta* **2006**, *51*, 3551.
[64] M. F. Hurley, C. M. Efaw, P. H. Davis, J. R. Croteau, E. Graugnard, N. Birbilis, *Corrosion* **2015**, *71*, 160.
[65] M. Jönsson, D. Thierry, N. LeBozec, *Corros. Sci.* **2006**, *48*, 1193.
[66] K. A. Yasakau, M. L. Zheludkevich, S. V. Lamaka, M. G. S. Ferreira, *Electrochim. Acta* **2007**, *52*, 7651.
[67] D. Klotz, *Electrochem. Commun.* **2019**, *98*, 58.
[68] J. Chen, J. Wang, E. Han, J. Dong, W. Ke, *Electrochim. Acta* **2007**, *52*, 3299.
[69] A. D. King, N. Birbilis, J. R. Scully, *Electrochim. Acta* **2014**, *121*, 394.
[70] L. Y. Cui, R. C. Zeng, S. Q. Li, F. Zhang, E. H. Han, *RSC Adv.* **2016**, *6*, 63107.
[71] J. Dong, Y. Ozaki, K. Nakashima, *J. Polym. Sci. Pol. Phys.* **1997**, *35*, 507.
[72] J. Dong, Y. Ozaki, K. Nakashima, *Macromolecules* **1997**, *30*, 1111.

SUPPORTING INFORMATION

Additional supporting information may be found in the online version of the article at the publisher's website.

How to cite this article: C. Das, E. Kastania, J. Witt, O. Ozcan, *Mater. Corros.* **2021**, 1–9. https://doi.org/10.1002/maco.202112708